Interpretation of oxygen profiles in the aftermath of the BP/Deepwater Horizon hydrocarbon discharge

Christof Meile[1], Ming-Jun Lai[2], Annalisa Bracco[3], Hao Luo[3] and Samantha Joye[1]

[1] Department of Marine Sciences, University of Georgia, Athens, GA 30602. Email: cmeile@uga.edu, mjoye@uga.edu

[2] Department of Mathematics, The University of Georgia, Athens, GA 30602. Email: mjlai@math.uga.edu

[3] Earth and Atmospheric Sciences, Georgia Institute of Technology, Atlanta, GA 30332. Email: annalisa@eas.gatech.edu, hao.luo@eas.gatech.edu

submitted to Deep-Sea Research II

Abstract

In the aftermath of the BP/Deepwater Horizon hydrocarbon discharge in 2010, a subsurface plume characterized by hydrocarbon concentrations highly elevated above background and a drawdown of O_2 was documented in Gulf of Mexico deep water to the southwest of the wellhead. The magnitude of the O_2 deficit and the processes responsible were poorly constrained and remain a subject of debate. Here, we present an analysis of O_2 drawdown from two research cruises conducted near and to the southwest of the wellhead and introduce a novel interpolation method to quantify total O_2 consumption. We illustrate that accurate estimates of total O_2 depletion must account for water movement and, more importantly, must capture the spatial structure of the O_2 anomaly field, which is difficult with the sparse sampling regime typically utilized on oceanographic cruises. We further show that in late May/early June in the vicinity of the wellhead, increased oxygen anomalies correlate with increasing methane oxidation rates and distance from the wellhead, which reflects the exposure time of the microbial community to hydrocarbons.

Introduction

In 2010, the BP/Deepwater Horizon (DWH) discharge injected an unprecedented amount of hydrocarbons into Gulf of Mexico deep waters. Between April 20 and July 15, 2010, when the well was capped, up to 750,000 t of oil and 500,000 t of gas, mainly methane, was released into the Gulf's deep waters near the wellhead (Joye et al. 2011a). A central question to guide recovery activities and assess ecological impacts was the fate of those hydrocarbons injected into the water column. The majority (~70%) of oil buoyantly rose to the ocean surface (McNutt et al.

2011, Reddy et al. 2012), where hydrocarbons were removed from the sea surface by skimming, burning, exchange with the atmosphere. Some fraction was biodegraded (McNutt et al. 2011) and surface weathering and biological activity resulted in a substantial sedimentation to the seafloor, impacting benthic infauna and corals (White et al. 2012, Joye et al. in prep). A fraction of the hydrocarbons ejected from the wellhead – at least 30% - partitioned into the water column, forming subsurface plumes (Diercks et al. 2010, Camilli et al. 2010).

Such subsurface plumes observed at water depths between 700 and 1300 m had been predicted by modeling (Jøhansen et al. 2001, Socolofsky et al. 2011), and attracted broad attention since the fate and impact of oil and dissolved gas at such great depths is difficult to quantify. Physical ocean models available in 2010 were limited in their ability to predict the fate of the subsurface plumes, likely due to insufficient resolution, and to the limited predictability of deepwater transport in most of the Gulf of Mexico (Cardona and Bracco 2013). However, injection of labile carbon at depth in the ocean clearly increased rates of aerobic microbial metabolism, raising concerns about possible O_2 depletion in the water column. If this metabolic O_2 consumption occurred at a rate faster than O_2 replenishment via physical transport, O_2 concentrations could have been drawn down to levels harmful for marine life.

As a consequence, identifying the magnitude and loci of O_2 drawdown as well as quantifying the physical processes resupplying O_2 are important tasks; such information will help elucidate the factors that control the extent of O_2 depletion. Kessler et al. (2011) linked O_2 drawdown explicitly to the oxidation of methane. Joye et al. (2011b) challenged this interpretation, citing significant uncertainties in the mass balance, poor constraints on the model presented, and ambiguity in the microbial data, which limited the identification of clear trends in microbial evolution between the reported June and September sampling campaigns. Undoubtedly, without direct measurements of microbial abundance and activity, pinpointing the timing of microbial blooms is challenging (see e.g. Valentine et al. (2010), who argued that 70% of O_2 consumption in fresh plumes was due to microbial oxidation of propane; Kessler et al. (2011), who argued for a peak in methane oxidation for the beginning of August; Du and Kessler (2012), who indicate maxima in hydrocarbon oxidation in mid July; Valentine et al. (2012), who suggest peak non-methane hydrocarbon oxidation for mid June to early July). For example, the presence of gas hydrates in deepwater plumes – which were not considered in the above analyses – can affect dissolved gas dynamics and alter dissolved gas ratios (Joye et al. 2011a), complicating the identification of the underlying causes for observed changes in concentrations based on gas ratios or isotopic shifts alone (Valentine et al. 2010). Direct measurements of methane oxidation rates in May and June 2010 revealed that methane oxidation rates ramped up quickly and declined after mid-June (Crespo-Medina et al. 2014), showing that the proposed propane priming of hydrocarbon metabolism (Valentine et al. 2010) did not apply to methane oxidation.

Here, we revisit some of the mass balance considerations, which were used to equate the amount of O_2 drawdown to the amount of gas injected in the Gulf of Mexico deep water assuming complete oxidation. Working with the observational data from the Pisces IV cruise, which sampled the water column SW of the Macondo site in late August/early September, we focus on three questions: (1) How sensitive is the estimate of the O_2 anomaly – the O_2 missing compared to natural background - to the method used in the data interpolation? (2) How important is it to account for fluid flow during the research cruise on which measurements were taken? (3) How sensitive are the O_2 consumption estimates to scale variability (e.g. scales smaller than those sampled)? To address these questions, we present a novel bivariate spline methodology, correct sampling conditions to a common date using high resolution flow fields generated by an ocean circulation model, and reanalyze high-resolution model results by Valentine et al. (2012) that simulate O_2 drawdown in the Gulf of Mexico deep water. Finally, to compare metabolic processes to O_2 drawdown, we present data from the Walton Smith research cruise at the end of May 2010 near the Deepwater Horizon wellhead, for which both O_2 profiles and methane consumption rates were measured.

Methods

Data

O_2 anomalies from O_2 profiles. Data collected on an R/V Pisces expedition (20 August – 2 September, 2010) SW of the Macondo well was obtained from the National Oceanographic Data Center (http://data.nodc.noaa.gov/DeepwaterHorizon/Ship/Pisces/ORR/Cruise_04/); 133 water column hydrographic profiles were analyzed to O_2 concentration calculate drawdown (Fig. 1; 26.3 to 29.3N and 87.3 to 92.8W). Hydrographic profiles (n=88) from the R/V Walton Smith expedition (May 26 – June 6, 2010) were obtained from http://data.bco-dmo.org/jg/dir/BCO/DWH_Deep_Microbes/. Oxygen anomalies were quantified by manually curating measured profiles and identifying O_2 depletion against background concentrations in approximately 1 m depth intervals between 700 and 1300 m water depth. Oxygen deficits were estimated in each profile by first identifying the region with a distinct drop below the natural smooth convex concentration profile. Then, within this range, the anomaly was quantified as the

difference of the measured concentration from a linear background. This linear rather than a convex down estimate of the background O_2 in the depth-interval between top and bottom of the depth range results in a conservative estimate of the anomaly.

O_2 anomalies from Valentine et al. (2012). Oxygen anomalies for 1000 to 1300 m water depth were extracted from Movie S2 provided in Valentine et al. (2012), who simulated the evolution of O_2 drawdown between 87.5 - 89.5°W and 27.3 - 29.3°N for 150 d starting in April 23, 2010. In the Valentine et al. model, flow fields were computed with a circulation model with a horizontal resolution of 0.04° (approximately 4 km) and 20 layers in the vertical. Daily flow fields and hydrocarbon input rates were then used in concert with a comprehensive description of O_2 consumption due to hydrocarbon consumption and bacterial growth. We used frames 370 to 2807 with a step interval of 25, which provided daily snapshots. After masking land, seafloor and the symbols marking the location of the well head and measurements, the color indicating O_2 depletion was translated into concentrations, using the color information given in the scale bar, with a minimum threshold of 0.8 μM. To assess the role of heterogeneity below the sampling scale, the simulation domain was divided into 20 by 20 rectangular subdomains, which approximates the sampling density of the Pisces IV data set. Then, from each of these quadrants a point location was selected at random, thus representing an artificial data set comparable to the measured one. These artificial data sets were then used for interpolation by kriging (see below) to every single pixel location to quantify the total O_2 anomaly.

Methane concentration and oxidation rate measurements. Water samples for methane concentration and oxidation rate quantification were obtained from Niskin bottles attached to the

CTD rosette and tripped at specific depths to capture the dynamics of the deepwater plume. Samples for dissolved methane and alkane concentration quantification were collected as described previously (Joye et al. 2011a). Alkane concentrations were determined using headspace extraction, followed by gas chromatography for quantification. A 0.25 to 1 mL headspace sub-sample was injected into a gas chromatograph (SRI model 8610C) equipped with a flame ionization detector and a temperature ramp was employed to higher alkanes. Concentrations were calculated by comparison to a certified mixed alkane standard (C_1 to C_5, Scott Specialty Gases®). Aerobic methane oxidation rates were measured using a tritiated (^3H) CH_4 radiotracer technique (Carini et al. 2005). Reactions were done in triplicate for each depth in gas-tight glass vials. A 100 µl aliquot of the C^3H_4 tracer solution was injected into each replicate (tracer activity = 2 kBq; the amount of methane added via tracer addition was less than 3 nM, compared to 100's of µM methane available in situ). Killed controls were amended with 3.7% formaldehyde prior to tracer addition. Samples were incubated at in situ temperature for 24 to 48 hours; linearity of activity was confirmed by time series. Reactions were terminated by adding 20% (vol:vol) of reagent grade ethanol to each vial. Labeled C^3H_4 was removed by purging the sample with hydrated methane for at least 30 minutes. Scintillation cocktail (ScintiSafe Gel®) was then added to a sub-sample (750 µL) and ^3H_2O produced was quantified using a Beckman 6500 liquid scintillation counter.

Flow dynamics

To account for advective water movements over the duration of the sampling period, we used the velocity field generated by a regional simulation of the Gulf of Mexico circulation. The model adopted is ROMS (Regional Ocean Modeling System; Marchesiello et al. 2003); we implemented the ROMS-Agrif 2.1 version (Debreu et al. 2012). The integration was performed over the whole Gulf on a 5 km horizontal resolution grid (parent grid) with a two-way nested domain (child grid) where resolution increased to 1.6 km between [96.31° -86.93° W] and [25.40° - 30.66° N], covering the area of the Pisces IV cruise track. The model contained 70 terrain-following layers, with no less than 30 layers within the upper 500 m and enhanced resolution in the bottom 500 m. The model bathymetry was derived from Etopo2v2 and was smoothed using a Shapiro smoother (Penven et al. 2008) to ensure negligible pressure gradient errors. ERA-Interim (Dee et al. 2011) 6-hourly surface momentum fluxes and daily heat fluxes forced the model from 2009 onward. At the open boundaries of the parent domain, ROMS was nudged to the monthly varying barotropic velocity fields of the HYCOM NCODA hindcast (Chassignet et al. 2003; Cummings 2005) available at http://hycom.org/dataserver/goml0pt04/expt-30pt1. Initial conditions were provided by a 20-year long, stationary simulation forced by ERA-Interim monthly climatological averages calculated over the period 1992-2012. This model configuration provides an excellent representation of the circulation and density structure of the Gulf of Mexico, particularly in the nested area, improving on that described by Cardona and Bracco (2013).

In the 700-1300 m depth horizon of the subsurface plume, the flow was predominantly horizontal over the 2-week sampling period. The modeled vertical velocity field at those depths was associated, to a large extent, to near inertial and superinertial motions (Zhong and Bracco 2013) and did not generate significant diapycnal mixing on the time scales considered. Thus, the modeled horizontal velocity field at 1100 m water depth was adopted to estimate the impact of advective displacement of water parcels. Using 12-hour averages of the horizontal velocities, u and v, the position of the sample locations was corrected for horizontal flow to midpoint through the observational window on August 26:

$$\binom{x}{y}_{new} = \binom{x}{y}_{old} + \binom{u}{v} dt \quad (1)$$

where dt was set to 1200 s for particle tracking forward in time, and -1200 s if the sampling time was later than half way through the cruise and the station locations were advected backward in time. At each time step, the velocities u and v were linearly interpolated in space and time to the current time and position. Horizontal mixing coefficients are poorly constrained, and therefore the effect of mixing on the lateral distribution of O_2 anomalies was ignored. Vertical exchanges are also difficult to estimate, and as in previous studies, e.g., Valentine et al. (2012), are not accounted for herein. Therefore, the interpolation of the flow-adjusted anomalies was performed only on the depth-integrated anomaly values.

Interpolation

Amongst the large variety of interpolation methodologies (e.g. Myers 1994, Li and Heap 2011), we used ordinary kriging and a novel bivariate spline method to quantify O_2 depletion in the Gulf of Mexico deep water. Interpolation was performed both on depth-integrated O_2 deficits, computed by simple summation and multiplication by the layer thickness, and on a layer-by-layer basis, using the average O_2 concentration deficit within the layer at any given location.

Kriging. Assuming no trend in O_2 anomalies over the domain, we employed ordinary kriging. Latitude and longitude information was first transformed into metric distances (Kleder 2005). Variograms were generated with 50 bins and fitted with an exponential model with a zero nugget-value using the implementation of Schwanghart (2010a,b). Interpolation was performed using the implementation of Schwanghart (2010c) to the same triangulation as used for the bivariate splines.

Bivariate splines. To approximate the O_2 anomalies, we adopted piecewise bivariate polynomial functions over a triangulation (bivariate splines; for theory and computation see Lai and Schumaker (2007), Awanou et al. (2006), Lai and Meile (2014)). The triangulation was based on the sampling locations, with additional nodes added (Fig. 1), and we used bivariate splines of degree d=5 and smoothness r=1. Our computation started with discontinuous piecewise polynomial functions over the triangulation, setting the smoothness conditions between two neighboring triangles (sharing an interior edge) together with interpolation conditions and non-negativity conditions as side constraints. The minimization problem was solved using a thin-plate energy functional. Formally, the interpolated anomaly S_j was computed such that

$$S_j = \arg min_{s \in S_d^r(\Delta)} \begin{cases} E(s), s(x_i, y_i) = o_{i,j}, i = 1, \dots, n \\ s(x, y) \geq 0, (x, y) \in \Omega \end{cases} \tag{2}$$

where $S_d^r(\Delta)$ is the bivariate spline space of degree d, smoothness $r \geq 1$ with $d > r$ over triangulation D, s denotes the splines, x and y indicate latitude and longitude, respectively, $o_{i,j}$ denotes the observation in profile i at depth j, and $E(s)$ is the thin-plate energy functional

$$E(s) = \int_\Omega \left(|D_x^2 ss|^2 + 2\left|D_{xx} D_y \; ss\right|^2 + \left|D_y^2 ss\right|^2 \right) dxdy \tag{3}$$

where $\Omega = \cup_{T \in \Delta} T$ is the union of all triangles in Δ, D_x, D_y = derivatives along x and y direction, respectively, and the O_2 anomaly is assumed to be continuously differentiable. Each spline function is given by

$$s(x,y) = \sum_{i+j+k=d} c^t_{ijk} B^t_{ijk}, if\ (x,y) \in t \in \Delta \quad (4)$$

where $B^T{}_{ijk}$ are Bernstein-Bézier polynomials of degree $i+j+k = d$ (see Chapter 2 in Lai and Schumaker 2007), and the coefficient vector $\mathbf{c}$=($c^t_{ijk}, i+j+k = d, t\ in\ \Omega$) of size ($N(d+1)(d+2)/2) \times 1$, where N is the number of total triangles in Δ.

Non-negativity of the O_2 anomaly was ensured using a side constraint $\mathbf{c} \geq 0$. Combining smoothness $\boldsymbol{H}\mathbf{c}$=0, non-negativity and matching the measured values results in the following constrained minimization problem:

$$\min\{\mathbf{c}^T\mathbf{E}\mathbf{c}, \boldsymbol{H}\mathbf{c} = 0, \boldsymbol{I}\mathbf{c} = \mathbf{o}_{\boldsymbol{j}}, \mathbf{c} \geq 0\}, \quad (5)$$

where $\boldsymbol{E}$ is the symmetric and nonnegative definite matrix associated with the thin-plate energy functional $E(s)$, i.e. $\mathbf{c}^T\mathbf{E}\mathbf{c} = E(s)$. The corresponding unconstrained minimization

$$\min_{\mathbf{c}\geq 0} J(\mathbf{c}) \quad (6)$$

with

$$J(\mathbf{c}) = \mathbf{c}^T\mathbf{E}\mathbf{c} + \alpha \parallel \boldsymbol{H}\,\mathbf{c}\|_2^2 + \beta\ \|\boldsymbol{I}\,\mathbf{c} - \mathbf{o}_{\boldsymbol{j}}\|_2^2, \quad (7)$$

where α and β are weighting parameters, was solved using a classic Uzawa algorithm, which converges for elliptic minimizing functionals such as $J(\mathbf{c})$ (Ciarlet 1989), starting with an initial guess S^0 , a penalized least squares spline fit of the values $\mathbf{o}_{\boldsymbol{j}}$, and initial parameter vector $\lambda^{(0)}$ = $\mathbf{1}$, where $\mathbf{1}$ is a vector with 1 in all entries. For $k \geq 1$, we iteratively minimized the following quadratic function with a fixed parameter $\alpha > 0$ and $\beta = 1$

$$\min_{\mathbf{c}}\left(J(\mathbf{c}) - < \lambda^{(k)}, \mathbf{c} >\right) \quad (8)$$

to find $\mathbf{c}^{(k)}$ and update

$$\lambda^{(k+1)} = \max\{\lambda^{(k)} - \rho(\mathbf{c}^{(k)}), 0\}, \tag{9}$$

where $< \lambda^{(k)}, \mathbf{c} >$ stands for inner product of two vectors $\lambda^{(k)}, \mathbf{c}$, $\rho > 0$ is a step size. We implemented this algorithm in MATLAB and an initial ρ of 10^{-5} which is reduced if not converging. Simulations were performed with α set to 10^{-2} to 10^{-8}, selecting the solution with no negative concentrations and the smallest relative error.

Results and Discussion

Below, we address the questions on the importance of interpolation methodology, the impact of profile data averaging, and the effect of the temporal offset between sampling events using the Pisces IV data set. We then quantify the uncertainty of O_2 deficit estimates due to the sparsity of the data, and discuss the relationship between measured process rates and observed O_2 deficits during the Walton Smith cruise.

Test of the bivariate spline algorithm. The bivariate spline based interpolation balances smoothing with fitting to the data. To test the performance of our algorithm, it was applied to the high-resolution model simulations of O_2 anomalies of Valentine et al. (2012). We arbitrarily selected a small patch from July 18 (Fig. 2) and adjusted the relative importance of smoothing vs. data fitting in the interpolation (Eq. 6) by varying α to match model results. Standard deviations were minimal for α-values of 10^{-8} or smaller. The non-negativity constraint embedded in the bivariate spline method ensured that the spline fitted the non-negative O_2 anomaly data without producing negative anomalies, i.e O_2 concentrations that significantly exceeded the true O_2 values. The bivariate spline method did not exhibit over- and under shooting of the measured data, leading to physically sound results.

Impact of interpolation method. When quantifying O_2 depletion in the Gulf of Mexico (GoM) deep water based on the data collected on Pisces IV in August 2010, ordinary kriging resulted in a semi-variogram that was fitted using an exponential model with a sill of 454 $g^2\ m^{-4}$ and a range of 14.5 km for the depth-integrated anomalies, which is about 2.5 times the typical distance between sampling locations. The total O_2 deficit within the area covered by the measurements resulting from kriging was 0.76 Tg. The bivariate splines worked well for $\alpha = 10^{-4}$, resulting in an estimated total O_2 drawdown of 0.73 Tg. Thus, the numerical results showed a reasonable agreement between the bivariate spline method and ordinary kriging, and both revealed the presence of a number of discontinuous areas with substantial O_2 drawdown (Fig. 3).

The finding that the magnitude of the O_2 anomaly does not depend strongly on the method of interpolation is consistent with Kessler et al. (2011) who obtained similar results when using kriging, minimum curvature, natural neighbor, radial basis function or triangulation as contouring methods. Because of the uncertainty introduced by estimating O_2 deficits outside the area covered by the observations, no stringent comparison with the results from Kessler et al. (2011) was performed. However, when using a domain approximating theirs, our reanalysis yielded results similar to the higher end of the 0.96-1.25 Tg O_2 range reported there.

Kriging by layer vs. the use of depth-integrated data. The three-dimensional distribution of O_2 anomalies was patchy and the water depth of the maximum O_2 depletion within a profile varied (see visualization in Fig. 1 of Joye et al. 2011b). Thus, quantifying the mass deficit by integrating the interpolated O_2 anomalies determined from depth-integrated data may not yield the same result as interpolating the data layer-by-layer and then summing up the contributions from each depth segment. This variation with depth is reflected in the kriging range, which for layers with significant O_2 anomalies varied between 6.6 and 21.1 km. Comparison of the result from interpolating depth-integrated data versus the integration of kriging interpolations for individual 10-m thick layers indeed revealed a difference, albeit a negligible one (2%; 0.76 vs. 0.77 Tg).

Effect of horizontal flow. For samples taken at different times, the observed spatial patterns may reflect transport processes, rather than an instantaneous snapshot of O_2 anomalies, or a combination of the two. We aimed at quantifying the role of advection within the domain of the Pisces IV cruise by correcting the location of the sampling point for a reasonable estimate of the advective velocity to produce a spatial pattern at a given point in time. Here, the location of all stations was advected to their position mid point through the Pisces IV cruise on August 27.

Comparison of sampling and flow-adjusted locations shows that (modeled) lateral advection has only a small effect on the position of the sampling locations over the 2-week period considered (Fig. 1). Horizontal velocities at stations east of 89.5°W are generally small (≤ 0.02 m s^{-1}), characterized by a variance close to zero during the period considered, and directed towards E-NE. A line of small eddies with radius of about 8 km is found at approximately 87.5°W and between 27° and 29°N. Those eddies are continuously generated close to the continental slope, are both cyclonic and anticyclonic, and are characterized by rotational speeds reaching 0.05 ms^{-1}. West of 89.5°W and between 26.5° and 27°N two cyclones with radius of approximately 20 km induced higher velocities that were highly variable in time and space and topping 0.1 m s^{-1}, which were superposed onto a weaker (≤ 0.035 m s^{-1}), westward, terrain-following mean current. Summer mean current speeds and directions were consistent through the four years simulated (2009-2012). Eddy variability was always higher around 87.5°W (cyclones and anticyclones) and west of 90°W (cyclones only). Because of the overall limited translocation and relatively weak deep mean currents along the continental slope in the Gulf of Mexico, original and adjusted locations can visually be paired at all stations.

Consistent with the limited shift in locations (Fig. 1), the interpolation of the depth-integrated O_2 anomalies using kriging gives similar results with and without accounting for advection. Taking into account the movement of water parcels over the sampling period, the total O_2 drawdown is approximately 8% larger than when not accounting for changes in location. This indicates that the correction for horizontal advection is of minor magnitude in this setting.

Subgrid heterogeneity. The data set collected to trace the subsurface plume O_2 deficient water consisted of 133 profiles taken over a 2-week period, covering an area of about 50,000 km^2. Thus, despite the good coverage compared to more routine oceanographic sampling (where during a 2 week cruise, perhaps 40 profiles would be collected), this nonetheless represents sparse observational data. However, the quantification of the O_2 deficit using interpolation methods requires a data set that captures spatial structure of the true anomalies.

To assess whether variability at scales smaller than the sampling grid was captured in the Pisces data set, model simulations (Valentine et al. 2012) that provide O_2 anomalies at a much finer scale were queried. These simulations show a rather symmetric elliptic O_2 anomaly at the beginning, which by the end of May is much elongated and developed long tails by the end of July 2010 (e.g. Fig. 2). The model builds on a mechanistic description of the underlying transport and reaction processes and it is treated here as an accurate representation of the O_2 concentration field. It is noteworthy, however, that uncertainties are inherent in such complex models, e.g. arising from difficulty to appropriately parameterize the microbially-mediated reaction network, from the temporal and spatial resolution of the physical model, which, while better than what provided by in situ data coverage, is still limited, and to the poor predictability of deep flow mesoscale variability in Gulf (Cardona and Bracco 2013).

Reconstructing the O_2 drawdown from randomly selected data points at a density similar to the observational data allows one to assess how robust estimates of the total O_2 deficit are. The mean of 100 realizations, representing the equivalent of 100 distinct cruise tracks is in close agreement with the true value (compare squares and black line in Fig. 4). However, the uncertainty in the estimate of the O_2 deficit, reflected by the variability around the mean, is substantial over the entire time course, from the end of April to the end of July 2010, with a coefficient of variation of about 0.2. Such variability around the mean challenges the attribution of O_2 deficits to processes based on a mass balance alone.

Processes responsible for O_2 drawdown. To identify the processes responsible for the apparent O_2 drawdown in the deep water, we compared measured rates of methane oxidation from the Walton Smith cruise at the end of May/beginning of June 2010 to observed O_2 anomalies. Typical measured values of the rate constant k were on the order of 0.01 – 0.02 d^{-1} (k = 0.0189 ±

0.0182 d^{-1}). Maximum values were 0.082 d^{-1}, more than an order of magnitude higher than the estimates of Kessler et al. (2011) for the end of May 2010. The rate measurements revealed no correlation between *k* and the methane concentration or O_2 drawdown (not shown). However, the depths with the highest methane oxidation rate in each profile correlated with the increasing observed O_2 anomalies and increased with distance from the wellhead. This is illustrated in Figure 5, where the horizontal axis is the product of distance from the wellhead and the oxidation rate. A linear relationship is expected if, over the time of observation, the rate was constant and the flow was steady, with negligible eddy mixing, so that the distance from the wellhead reflected the time of exposure.

The samples that exhibit O_2 drawdown indeed show such a general trend. The flow velocity implied in this trend ($v_{estimated}$ = R/C*d, where R is the oxidation rate, C the O_2 anomaly and d the distance from the well head) is on the order of a few cm/s, qualitatively consistent with the results of the above-mentioned ocean circulation simulations. The convex up pattern seen in the samples from prior to the riser cut (dashed and dotted lines in Fig. 5, period of April 26-June 3) is consistent with a slight increase in metabolic activity over time, which would accompany a bloom in the methanotropic or oil-oxidizing bacterial community (Crespo-Medina et al. 2014 and Kleindienst et al. 2014, respectively). The samples collected after the riser was cut on June 3, 2010 (Fig. 5, solid circles) are characterized by comparatively high anomalies given the measured rates and sampling location. This is likely to reflect the change in flow dynamics from a jet-like input of hydrocarbons prior to the riser cut, forming the subsurface plume, to a mushroom-cloud-like emission scenario after the cut, when the directional velocity of the plume was reduced, leading to longer residence time near the wellhead.

Conclusions

The O_2 drawdown in the deep water of the GoM in the wake of the Deepwater Horizon oil spill has attracted considerable attention (Joye et al. 2011a, Kessler et al. 2011, Raloff 2011), both due to novelty of such observed features and the potential implication for the fate of hydrocarbons and ecosystem health (Joye et al. 2011b). Two central topics of interest were the quantification of the total O_2 anomaly, and the identification of the processes responsible for it, which would shed light on the factors controlling the extent of O_2 depletion and thus allow for predictions of the magnitude of these low O_2 regions.

Here, a novel approach to spatially interpolate between measurements using a bivariate spline methodology applied to the Pisces IV and the Valentine et al. (2012) data sets showed that the approach enforces non-negativity, and provides a close fit to the data. Results compare favorably to the estimates obtained with ordinary kriging. These results also show that the O_2 anomaly obtained from depth-integrated data is very similar to the deficit obtained when performing interpolation for distinct depth layers separately. Furthermore, accounting for the movement of water parcels over the duration of the cruise also did not alter estimates of the O_2 deficit to a large extent (8% difference). However, spatial distributions of O_2 anomalies estimated with a reaction transport model (Valentine et al. 2012) indicate heterogeneity at the scale below that resolved during the Pisces IV cruise, which hampers quantification of total O_2 depletion from sparse data and challenges quantitative estimates of O_2 deficit and methane consumption in the wake of the Deepwater Horizon oil discharge. This also emphasizes the difficulty to capture such subsurface plumes with traditional oceanographic observations and stresses the need for autonomous sampling devices such Lagragian drifters or instrumented AUVs deployed at plume depth and programmed to drift with the plume equipped with appropriate sensors.

To identify the processes responsible for O_2 drawdown, we focused on a data set collected near the wellhead, approximately 6 weeks after the start of the oil spill. For late May/early June at the plume depth of about 1150 m, we identified a correlation between the distance from the wellhead, the measured oxidation rate and the observed O_2 anomaly, suggesting the importance of the exposure time to high methane concentrations to oxidation rates. The implied flow velocities are in the same order of magnitude of the flow velocities computed with the ocean circulation model, albeit slightly higher. Thus, while this data set cannot constrain the importance of Macondo hydrocarbon oxidation in the plume far field, it suggests that near the wellhead, methane was an important factor for O_2 drawdown in the subsurface plume.

Acknowledgements. We would like to thank the scientists, crew and captain of the Pisces IV and Walton Smith cruises. This work was supported by the NOAA Award NA07AR4300464 to the National Institute for Undersea Science and Technology (SJ), the National Science Foundation (OCE-1043225 to SJ) and the Gulf of Mexico Research Initiative “Ecological Impacts of Oil and Gas Inputs to the Gulf (SJ, AB and CM). This is ECOGIG contribution #214 and the Pisces IV and Walton Smith data reflect GRIIDC accession numbers R1.x132.134:0056 and XXX, respectively.

References

Awanou, G., Lai, M.J. and Wenston, P. 2006. The multivariate spline method for numerical solution of partial differential equations, wavelets and splines. G. Chen and M. J. Lai (eds.) Nashboro Press. pp. 24–74.

Camilli, R., Reddy, C.M., Yoerger, D.R., Van Mooy, B.A.S., Jakuba, M.V., Kinsey, J.C., McIntyre, C.P., Sylva, S.P. and Maloney, J.V. 2010. Tracking hydrocarbon plume transport and biodegradation at Deepwater Horizon. Science 330: 201-204.

Cardona, Y. and Bracco, A. 2013. Predictability and mesoscale circulation throughout the water column in the Gulf of Mexico. Deep-Sea Research II, in press.

Carini, S.A., G. LeCleir, N. Bano, and Joye, S.B. 2005. Activity, abundance and diversity of aerobic methanotrophs in an alkaline, hypersaline lake (Mono Lake, CA, USA). Environmental Microbiology 7(8): 1127-1138.

Chassignet, E.P., Smith, L.T., Halliwell, G.R. and Bleck, R. 2003. North Atlantic simulation with the HYbrid Coordinate Ocean Model (HYCOM): Impact of the vertical coordinate choice, reference density, and thermobaricity. J. Phys. Oceanogr. 33: 2504-2526.

Ciarlet, P. 1989. Introduction to numerical linear algebra and optimization. Cambridge University Press. 436p.

Crespo-Medina, M., Meile, C.D., Hunter, K.S., Tavormina, P., Diercks, A.R., Asper, V., Chanton, J.P., Shiller, A.M., Joung, D.J., Battles, J.J., Montoya, J., Villareal, T., Wood, M., Amon, R., and Joye, S.B. 2014. The rise and fall of methanotrophy following a deepwater oil-well blowout. Nature Geoscience (accepted).

Cummings, J.A. 2005. Operational multivariate ocean data assimilation. Quart. J. Royal Met. Soc., Part C: 131(613), 3583-3604.

Debreu, L., Marchesiello, P., Penven, P., and Cambon, G. 2012. Two-way nesting in spill-explicit ocean models: Algorithms, implementation and validation. Ocean Modelling 49-50: 1-21.

Dee, D.P., Uppala, S.M., Simmons, A.J., Berrisford, P., Poli, P., Kobayashi, S., Andrae, U., Balmaseda, M.A., Balsamo, G., Bauer, P., Bechtold, P., Beljaars, A.C.M., van de Berg, L., Bidlot, J., Bormann, N., Delsol, C., Dragani, R., Fuentes, M., Geer, A. J., Haimberger, L., Healy, S.B., Hersbach, H., Hólm, E.V., Isaksen, L., Kållberg, P., Köhler, M., Matricardi, M., McNally, A.P., Monge-Sanz, B. M., Morcrette, J.-J., Park, B.-K., Peubey, C., de Rosnay, P., Tavolato, C., Thépaut, J.-N. and Vitart, F. 2011. The ERA-Interim reanalysis: configuration and performance of the data assimilation system. Quart. J.Royal Meteorol. Soc. 137: 553–597. doi: 10.1002/qj.828

Diercks, A.R., Highsmith, R.C., Asper, V.L., Joung, D., Guo, L., Zhou, Z., Shiller, A.M., Joye, S.B., Teske, A.P., and Lohrenz, S.E. 2010. Characterization of subsurface polycyclic aromatic hydrocarbons at the Deepwater Horizon site. Geophysical Research Letters, 37, L20602, doi:10.1029/2010GL045046.

Du, M. and Kessler, J.D. 2012. Assessment of the spatial and temporal variability of bulk hydrocarbon respiration following the Deewater Horizon Oil spill. Env. Sci. Technol. 46(19): 10499507.

Johansen, Ø., Rye, H., Melbye, A.G., Jensen, H.V., Serigstad, B. and Knutsen, T. 2001. Deep Spill JIP – Experimental discharges of gas and oil at Helland Hansen – June 2000, Technical Report. SINTEF Applied Chemistry, Trondheim, Norway. 159p.

Joye, S.B., MacDonald, I.R., Leifer, I. and Asper, V. 2011a. Magnitude and oxidation potential of hydrocarbon gases release from the BO oil well blowout. Nature Geoscience 4: 160-164.

Joye, S.B., Leifer, I., MacDonald, I.R., Chanton, J.P., Meile, C.D., Teske, A.P., Kostka, J.E., Chistoserdova, L., Coffin, R., Hollander, D., Kastner, M., Montoya, J.P., Rehder, G., Solomon, E., Treude, T. and Villareal, T.A. 2011b. Comment on a persistent oxygen anomaly reveals the fate of spilled methane in the deep Gulf of Mexico. Science 332: 1033–1034.

Joye, S.B., Passow, U., Medeiros, P.M., Crespo-Medina, M., Montoya, J., Asper, V. and Diercks, A. 2014. Rapid sedimentation pulses impacted the seafloor in the wake of the Macondo Blowout. Proc. Nat. Acad. Sci. (in prep)

Kessler, J.D., Valentine, D.L., Redmond, M.C., Du, M., Chang, E.W., Mendes, S.D., Quiroz, E.W., Villanueva, C.J., Shusta, S.S., Werra, L.M., Yvon-Lewis, S.A. and Weber, T.C. 2011. A persistent oxygen anomaly reveals the fate of spilled methane in the deep Gulf of Mexico. Science 331: 312–315

Kessler, J.D., Valentine D.L., Redmond, M.C., and Du, M. 2011. Response to comment on "A persistent oxygen anomaly reveals the fate of spilled methane in the deep Gulf of Mexico". Science 332: 1033.

Kleder M. 2005. Convert lat, lon, alt to ECEF cartesian. http://www.mathworks.com/matlabcentral/fileexchange/7942-covert-lat-lon-alt-to-ecef-cartesian. MATLAB Central File Exchange. Retrieved Feb 2013.

Kleindienst, S. S. Grim, M. Sogin, M. Crespo-Medina, S.B. Joye, 2014. Rapid response time and striking sub-OTU diversity highlight the response of low-abundance microbial populations to the Deepwater Horizon oil spill. Proc. Nat. Acad. Sci. (submitted).

Lai, M.J. and Meile, C. 2014. Scattered data fitting with nonnegative preservation using bivariate splines and its application. Computer Aided Geometry Design (submitted).

Lai, M.J. and Schumaker, L.L. 2007. Spline functions over triangulations. Cambridge University Press. 592p.

Li, J. and Heap A.D. 2011. A review of comparative studies of spatial interpolation methods in environmental sciences: Performance and impact factors. Ecological Informatics. 6: 228-241.

Marchesiello, P., McWilliams, J.C., and Shchepetkin, A. 2003. Equilibrium structure and dynamics of the California Current System. J. Phys. Oceanogr. 33: 753-783.

McNutt, M, Camilli, R., Guthrie, G., Hsieh, P., Labson, V., Lehr, B., Maclay, D., Ratzel, A. and Sogge. M. 2011. Assessment of Flow Rate Estimates for the Deepwater Horizon / Macondo Well Oil Spill. Flow Rate Technical Group report to the National Incident Command, Interagency Solutions Group, March 10, 2011

Myers, D.E. 1994. Spatial interpolation: an overview. Geoderma 62: 17-28.

Penven, P., Marchesiello, P., Debreu, L., and Lefevre, J. 2008. Software tools for pre- and post-processing of oceanic regional simulations. Envir. Modelling & Software 23:660-662.

Raloff, J. 2011. BP spill's methane goes missing. Science News. January 29, 2011, p.11, http://www.sciencenewsdigital.org/sciencenews/20110129?pg=13#pg13.

Reddy, C.M., Arey, J.S., Seewald, J.S., Sylva, S.P., Lemkau, K.L., Nelson, R.K., Carmichael, C.A., McIntyre, C.P., Fenwick, J., Ventura, G.T., Van Mooy, B.A.S. and Camilli, R. 2012. Composition and fate of gas and oil released to the water column during the Deepwater Horizon oil spill. PNAS 109(50): 20229-20234. Doi:10.1073/pnas.1101242108.

Schwanghart, W. 2010a. Experimental (semi-) variogram. http://www.mathworks.com/matlabcentral/fileexchange/20355-experimental-semi-variogram. MATLAB Central File Exchange. Retrieved Feb 2013.

Schwanghart, W. 2010b. Variogramfit. http://www.mathworks.com/matlabcentral/fileexchange/25948-variogramfit. MATLAB Central File Exchange. Retrieved Feb 2013.

Schwanghart, W. 2010c. Ordinary kriging. http://www.mathworks.com/matlabcentral/fileexchange/29025-ordinary-kriging. MATLAB Central File Exchange. Retrieved Feb 2013

Socolofsky, S.A., Adams, E.E., and Sherwood, C.R. 2011. Formation dynamics of subsurface hydrocarbon intrusions following the Deepwater Horizon blowout. Geophysical Research Letters 38, L09602, doi:10.1029/2011GL047174.

Valentine, D.L., Kessler, J.D., Redmond, M.C., Mendes, S.D., Heintz, M.B., Farwell, C., Hu, L., Kinnaman, F.S., Yvon-Lewis, S., Du, M., Chan, E.W., Tigreros, F.G., and Villanueva, C.J. 2010. Propane respiration jump-starts microbial response to a deep oil spill. Science 330: 208-211.

Valentine, D.L. Mezic, I., Maešic, S., Crnjaric-Žic, N. Ivic, S., Hogand, P.J., Fonoberov, V.A. and Sophie Loire, S. 2012. Dynamic autoinoculation and the microbial ecology of a deep water hydrocarbon irruption. PNAS 109(50): 20286-20291.

White, H., Hsing, P., Cho, W., Shank, T.M., Cordes, E.E., Quattrini, A.M., Nelson, R.K., Camili, R., Demopolous, A., German, C.R., Brooks, J.M., Roberts, H.H., Shedd, W., Reddy, C.M. and Fisher, C.R. 2012. Impact of the Deepwater Horizon oil spill on a deep-water coral community in the Gulf of Mexico. Proc. Nat. Acad. Sci. 10.1073/pnas.1118029109.

Zhong, Y. and Bracco, A. 2013. Submesoscale impacts on horizontal and vertical transport in the Gulf of Mexico. 2013. J. Geoph. Res.-Oceans, vol. 118, 5651-5668, doi: 10.1002/jgrc.20402.

Figures

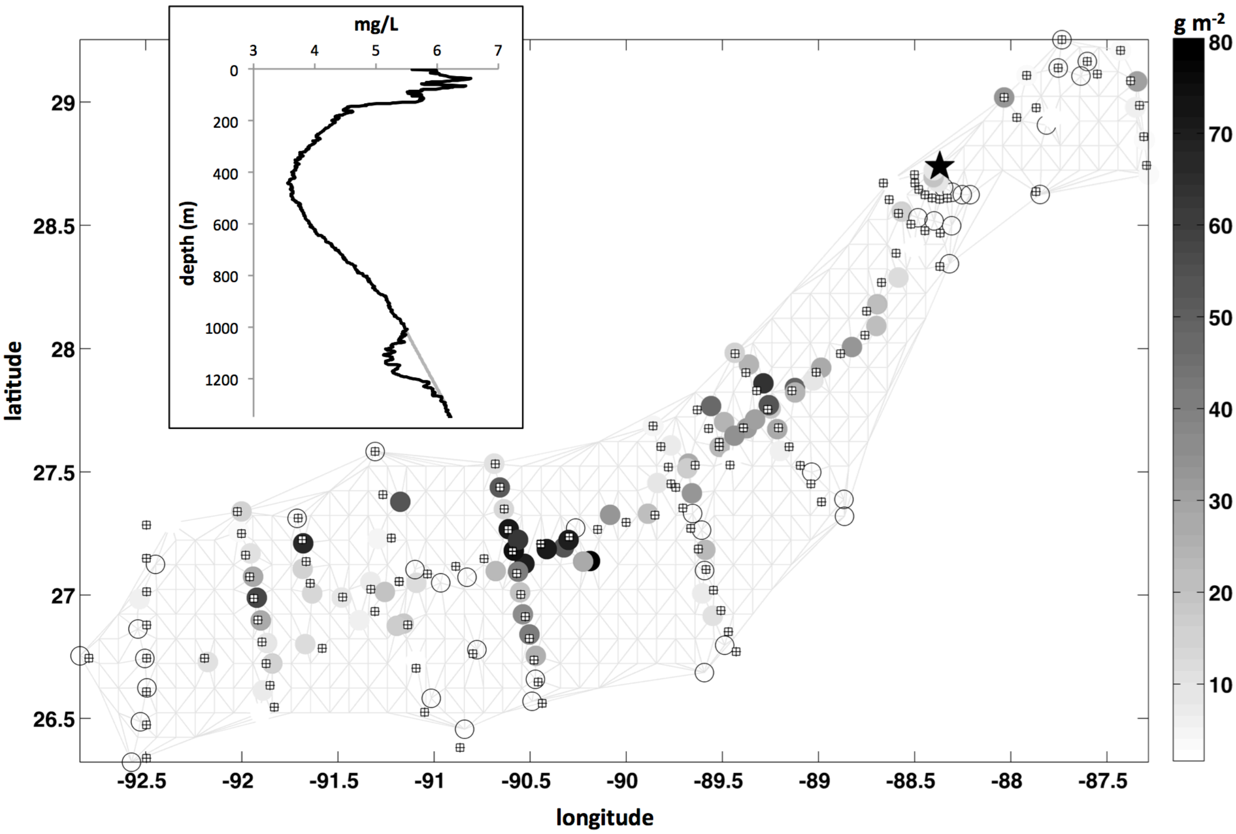

Figure 1. Depth-integrated O_2 anomalies in g m^{-2} established from measured concentration profiles. Crossed squares denote the location where the samples were taken, circles the reconstructed position of the water parcels at 1100 m water depth on August 26, mid point through the cruise. The magnitude of the O_2 anomaly is denoted by the gray scale of the circles. The light gray lines indicate the domain and mesh used with the moved locations. The black star indicates the position of the wellhead. The inset shows an example O_2 profile (black line) and the corresponding O_2 anomaly (difference between black and gray line).

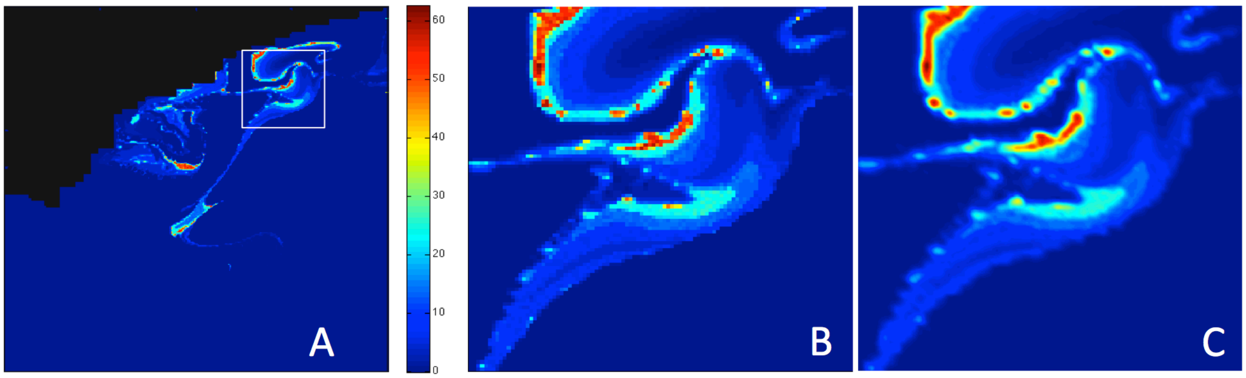

Figure 2. Simulated O_2 anomalies for July 18 in mM (A; Valentine et al. 2012). (B) and (C) show model data and spline reconstruction in the inset ($\alpha = 10^{-8}$). The large domain covers the area between 27.3 and 29.3°N and 87.5 and 89.5°W

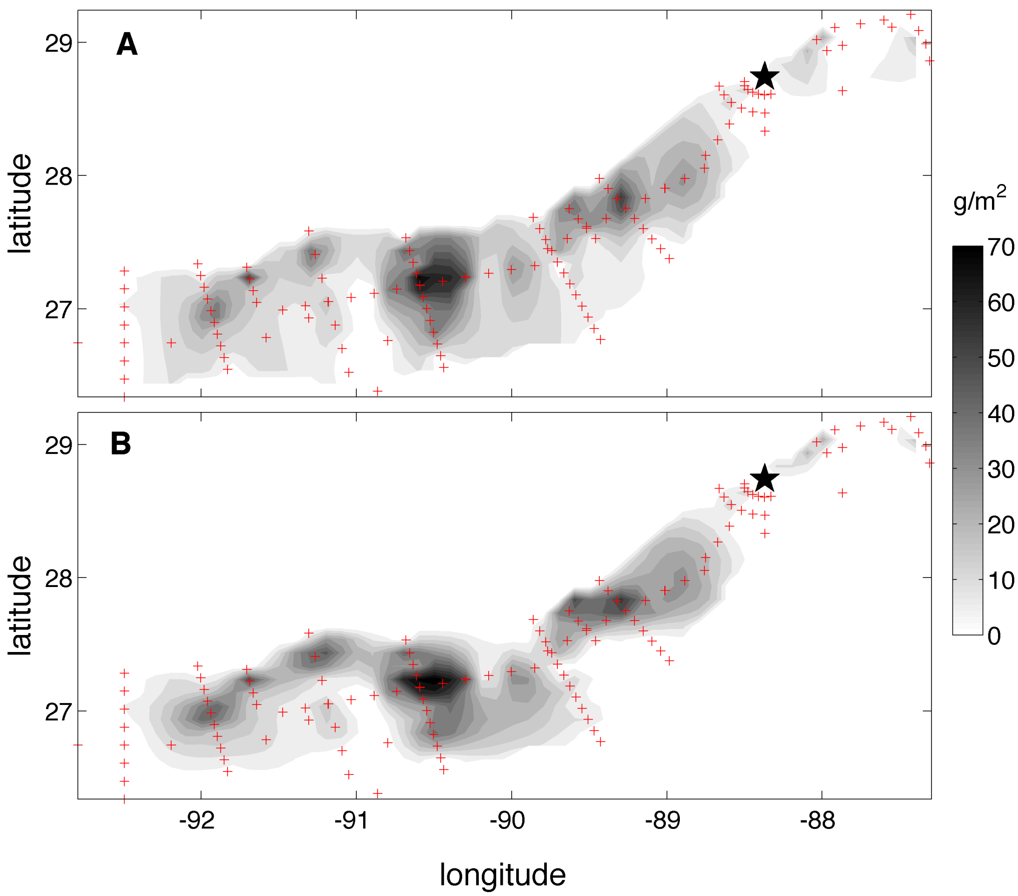

Figure 3. Contoured depth-integrated anomalies interpolated with kriging (A) and bivariate splines (B) using the original sampling locations indicated by crosses. The star is the wellhead location.

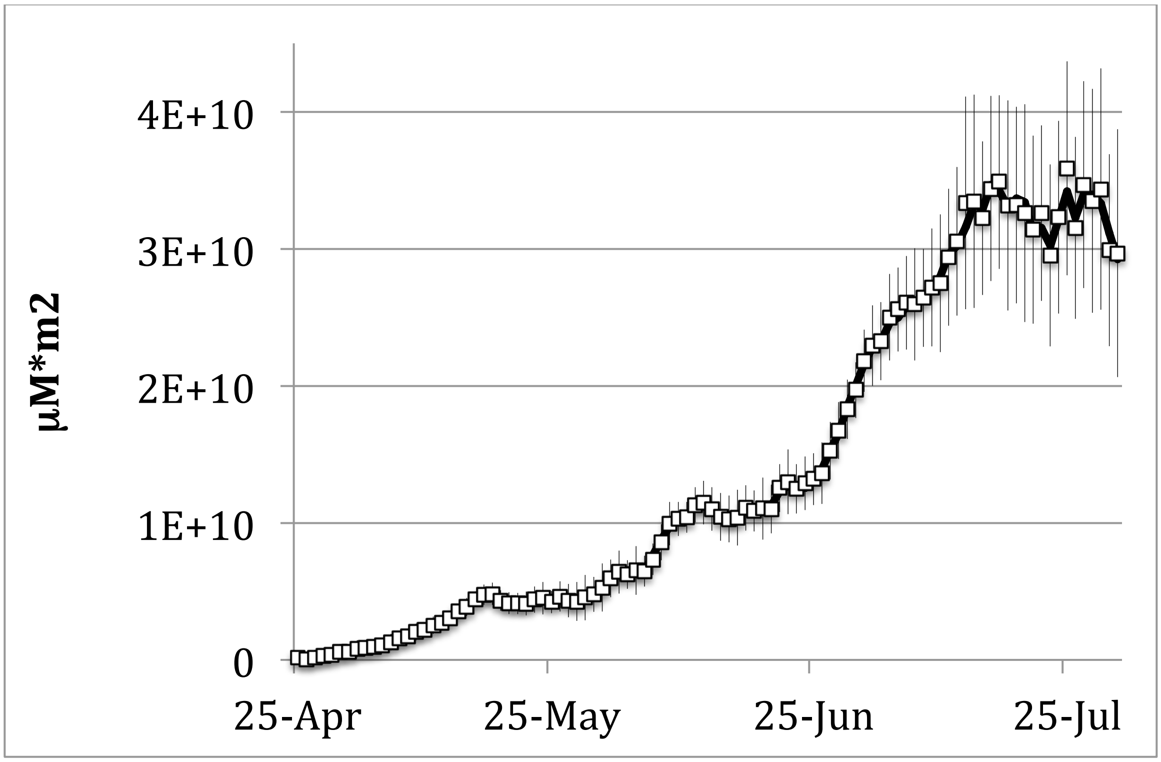

Figure 4. True (black line) and estimated mean (squares) O_2 deficit versus time. The vertical error bars denote one standard deviation, for 100 realizations, in which O_2 anomalies are extracted at random from the high-resolution model at a density comparable to the sampling density during Pisces IV, and then used to estimate the total O_2 deficit using ordinary kriging.

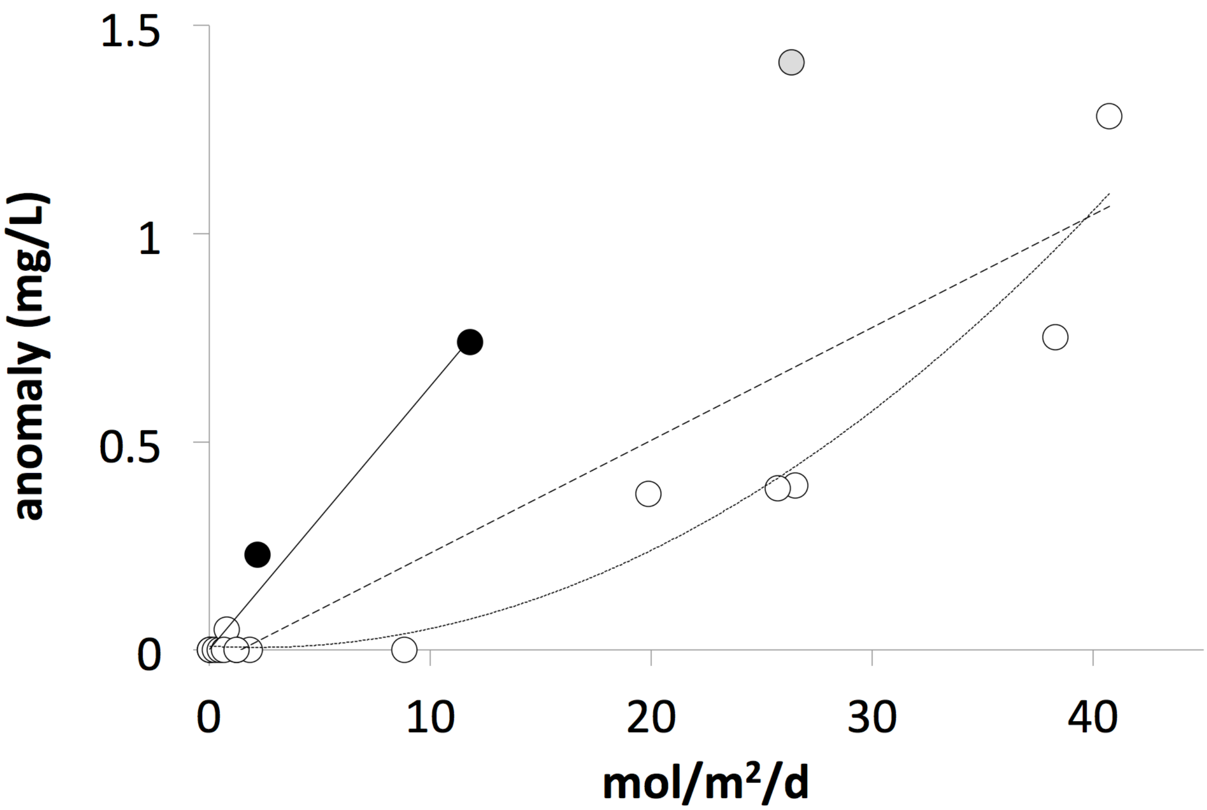

Figure 5. Distance from the wellhead times the measured rate of methane oxidation vs. the measured O_2 anomaly at the depth of the maximum methane oxidation rate in each profile. All data are from the Walton Smith cruise. Black and white/gray circles denote measurements before and after the riser was cut on June 3, 2010, respectively. The lines (line for after, before with (dashed line)/without (dotted line) the gray circle) reflect the fit with highest coefficient of determination.